Semiconductor Physics, Quantum Electronics & Optoelectronics, 2022. V. 25, No 4. P. 413-421.

Optics

Luminescent properties of cadmium sulfide nanocrystals grown from gas phase

A.B. Bogoslovska, D.O. Grynko, E.G. Bortchagovsky

V. Lashkaryov Institute of Semiconductor Physics, NAS of Ukraine, 41, prospect Nauky, 03680 Kyiv, Ukraine
E-mail: alla.bogoslovska@gmail.com

Abstract. Photoluminescent (PL) properties of undoped nanocrystals of cadmium sulfide were investigated as a function of excitation power intensity. Room-temperature PL spectra of CdS nanocrystals grown from the gas phase revealed two emission bands: with peak positions at 510 nm (near-band-edge emission) and close to 690 nm (deep trap defects). Tunable photoluminescence of CdS nanocrystals with the exchange of the main radiative channel from relaxation through defect levels to direct near-band-edge relaxation with the change of the color was demonstrated. Nonlinear behavior of the intensities of near-band-edge and defect level emission lines as well as the blue shift of the peak of defect level emission are discussed and explained by the finite capacitance of the defect subzone in the forbidden gap. The origin of the red-light emission is due to native defects such as sulfur vacancies or twinning interfaces.

Keywords: CdS, nanocrystal, photoluminescence, crystal morphology, excitation power.

https://doi.org/10.15407/spqeo25.04.413
PACS 68.70.+w, 71.55.Gs, 78.55.-m

Manuscript received 02.08.22; revised version received 31.10.22; accepted for publication 14.11.22; published online 22.12.22.

1. Introduction

Semiconductor nanostructured materials attract great scientific and technical interest, due to their unique properties and possibilities to create components for next-generation nanoscale electronic and optoelectronic devices. Today nanoscale semiconductor structures are widely used as essential components in such devices as photo-detectors [1, 2], light emission diodes [3, 4], laser [5], solar cells [6], sensors [7–9], optical switches [10], *etc*.

Ones of the most important functional nanostructures are quasi-one-dimensional (1D) semiconductors, namely: nanowires (NWs), nanobelts, nanorods, and nanotubes. Their unique properties are related to opportunity of rational and predictable synthesizing the single crystal forms with controlling all the key parameters, including chemical composition, size, shape, crystal structure and doping. Optical properties of nanostructures are very different from the respective bulk materials. Even beside quantum-size effects, high ratio of surface to the volume of such structures has big influence on luminescent and optical properties.

In recent years, many one-dimensional semiconductor nanomaterials, namely: ZnO [11], ZnS [12], GaN [13], InP [14] and InAs [15], have been intensively studied and proposed as active components to fabricate optoelectronic devices. II-VI compound semiconductors, especially cadmium chalcogenides, are the class of materials able to create 1D nanostructure, and they have been investigated in this form, too. These materials are recognized as the promising ones in optoelectronics owing to their high quantum efficiency and variable bandgap.

Among these semiconductors, CdS is one of the most important direct wide bandgap (about 2.5 eV, depending on the polytype [16]) semiconductors with the relatively high exciton binding energy ($29\text{ meV} \geq kT_{room}$) and exciton Bohr radius of approximately 2.85 nm. CdS nanostructures possess excellent electronic and optical properties owing to large optical absorption coefficients, high emission quantum efficiencies and the ability to tune emission in the visible range simply by changing its size or shape. For this reason, CdS nanostructures have been considered as the promising ones for photodetectors operating in the visible spectral range [17].

Today one-dimensional CdS nanostructures are synthesized using various approaches, including thermal evaporation [18], electrodeposition [19], template-assisted electrochemical synthesis [20], chemical vapor deposition [21], solvothermal methods [22], hydrothermal process [23], and vapor-liquid-solid growth (VLS) [24]. The most extensively employed methods to synthesize 1D nanostructures are vapor phase growth, since these methods give opportunities to grow nanostructures with high crystallinity, monodispersity, as well as controlled morphology and optical properties. In addition, this approach gives great opportunity for the bottom-up growth of complex structures.

The use of nanomaterials as building blocks for various optoelectronic devices requires sufficient control of their quality, because the intrinsic properties of semiconductor nanomaterials determined by the size, shape, and crystal structure are the important factors defining their optical properties. Also, a number of researches were performed to reveal the influence of strain, alloying and variable stoichiometry of 1D nanostructures on their optical and electric properties in order to widening the working range and flexibility of devices on the base of nanostructures [25–28].

One factor in manipulation of optoelectronic properties is the phase control of semiconductor NCs. CdS is well known to exist as two types of structural polymorphs, the cubic sphalerite or zinc blende (ZB) and the hexagonal wurtzite (WZ) structure. The bandgap is $E_g \cong 2.42$ eV for the bulk WZ phase and $E_g \cong 2.53$ eV for the bulk ZB phase [16]. Transformation of the crystal structure leads to the change of the bandgap, and, as a consequence, some variation of the optical properties of nanostructures [29–31].

In the previous work [32], we investigated the influence of technological growth parameters on the morphology and optical properties of CdS nanowires demonstrating correlation of the ratio of intensities of green near-band-gap and red defect/impurity luminescence with the quality of grown nanocrystals. This work is focused on investigation of the dependence of the photoluminescence emission of CdS nanocrystals with two types of structural polymorphs ZB and WZ as a function of the excitation power.

2. Experimental section

2.1. Sample preparation

Nanocrystals of CdS were synthesized using chemical vapor condensation by the technique of quasi-closed volume with hot walls. Decompositive sublimation of CdS powder in a high-temperature reactor inside a vacuum chamber was used as a vapor source. CdS powder was a semiconductor purity. Temperature of vapor source was 750 °C. Evacuation of silica reactor with graphite stages perfomed with criogenic sorption vacuum pump with the residual pressure in the chamber of $\sim 10^{-5}$ Torr. This technique allows growing single crystals of cadmium sulfide with a diameter from tens to hundred nanometers and the length up to millimeters, which is defined by the time of growth for both wurtzite and sphalerite type of symmetry. More detailed description of the technology was published earlier [32, 33].

Usually, the second source of additional sulfur vapor is used. It is known the thermodynamic equilibrium of A^2B^6 crystal with sulfur vapor to be shifted to creation of nonstoichiometric defects [34]. So, overpressure of sulfur vapor at the synthesis or during the following long-term annealing in sulfur vapors is used to decrease the defect concentration in crystals or films, what we used in our previous works [32, 35]. This approach decreased defectness of CdS nanocrystals remarkably. However the present work is aimed at investigation of the influence of defects on luminescent properties of nanocrystals. Thus, no additional source of sulfur vapor was used at the synthesis.

Nanocrystals used in the present investigation were grown on Mo glass slides as the substrate with gold seeds as nucleation centers. The gold nucleation seeds were prepared using deposition of a thin Au film with the thickness close to 2 nm on the substrate by thermal evaporation followed by annealing in vacuum. Film thickness during deposition was controlled by quartz microbalance and calculated through the mass uptake value.

2.2. Characterization

The growth and optical properties of CdS nanowires were investigated by X-ray powder diffraction (XRD), scanning electron microscopy (SEM), UV-visible photoluminescence (PL) spectroscopy.

SEM studies were performed using JEOL JSM35, JXA-8200. The phase composition of the films was analyzed by *ex-situ* X-ray diffraction carried out with a Philips X'Pert PRO X-ray diffractometer with CuKα radiation (λ = 0.154 nm). The qualitative phase analysis of the diffractogram was carried out using the ICDD database, PDF-2 Release 2012.

The optical properties of the material were investigated for ultraviolet-visible (UV-vis) photoluminescence at room temperature by using the automatic MDR-23 spectrometer (LOMO, USSR) with PMP-100 photomultiplier as a detector and a semiconductor laser with the wavelength 407 nm as the excitation source. Excitation power was regulated by a number of calibrated neutral filters. To ensure comparability of photoluminescence results, optical alignment was fixed during the measurements.

3. Results and discussion

The SEM image at low and high magnification of as-grown CdS nanocrystals ensemble is presented in Fig. 1. As it is seen in Fig. 1a, the large amount of CdS nanocrystals is distributed randomly on the substrate. Nanocrystals shown in Fig. 1b demonstrate bends distinctive for the change of the crystal polytype. It is apparent that the typical length of nanocrystals is in micrometer scale, and the diameter is in the scale of hundreds of nanometers. Some nanowires show a remaining catalyst gold dot on the top after growth, as it may be seen in Fig. 1c.

The phase structure and crystallinity of grown CdS nanocrystals were investigated using conventional X-ray diffraction. Fig. 2 shows the XRD pattern of as-synthesized CdS nanocrystals. The composition of nanocrystals is close to that in stoichiometric CdS with traces of Au catalyst and no byproduct peaks. It can be seen that the diffraction peaks correspond to the presence of both CdS structure phases. The ratio of cubic ZB to hexagonal WZ phase estimated using the method of corundum numbers is 59% to 41%, respectively. Gold is presented in the form of separated nanoparticles with cubic ZB structure. It is confirmed in Fig. 1c by electron microscopy demonstrating these nanoparticles at the end of freshly grown CdS nanocrystals [32].

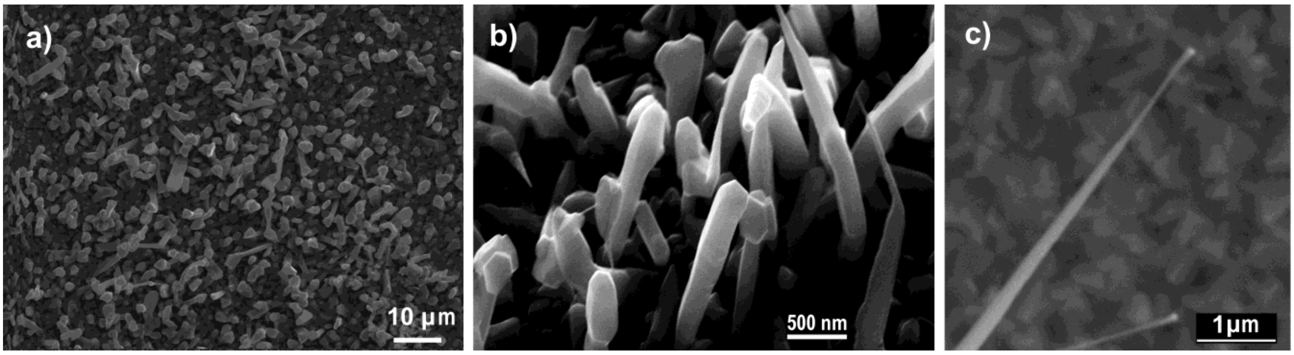

Fig. 1. Low (a) and high (b, c) resolution SEM images of as-prepared CdS nanocrystals. The panel (c) demonstrates residual gold dot at the end of grown CdS nanocrystals.

Photoluminescence of CdS nanocrystals was investigated at room temperature under the different excitation power changed by the set of neutral filters. All the shown in Fig. 3 PL spectra of CdS nanocrystals exhibit typical two emission peaks that originate from different excited states ascertained in numerous publications [32, 36, 37].

The high-energy band centered near 510 nm has a relatively narrow full-width at half-maximum (FWHM) close to 15 nm and is assigned to the near-band edge (NBE) emission. The origin of NBE can be related to one or both recombination kinds: free electron-hole or excitons or trapping the charge carriers by shallow states nearby the band edge [37, 38]. The broad emission peak ranging from 550 up to 800 nm is attributed to the radiative recombination of carriers on deep states in the forbidden band (defect level emission, DLE). It is typically associated with transitions related to sulfur vacancies (VS), interstitial cadmium, structure defects, trapped electrons/holes at surface defects [37, 39]. One more type of structural defects in the investigated samples can be electronic states induced by twinning interfaces in the CdS nanocrystals [40]. The FWHM of defect level emission is much larger than that of near-bandgap emission, which stems from defect complexes with slightly varying energy levels.

For better comparison, all the PL spectra measured for various excitation powers were normalized by the maximum intensity of DLE and plotted in Fig. 3b. At low excitation conditions (approximately 50 mW/cm^2), DLE gives the main contribution to luminescence of CdS NCs, because practically all the excited carriers are trapped by defect states within the forbidden band. The NBE emission has significantly, more than one order of magnitude, lower intensity. Due to the density of defect states is much lower than that of exciton-related near band-edge states, the intensity of DLE emission rises slower than that of NBE emission. At the increasing excitation power, the difference of PL intensities between DLE and NBE emissions becomes lower, and when the excitation power reaches its maximal value close to 21 W/cm^2, the PL intensity of the green NBE emission becomes dominant as it is seen in the corresponding spectra (Fig. 3b). The further increase in the excitation power makes NBE emission to be the main radiative channel.

This is clearly demonstrated by the PL spectra obtained under excitation of CdS nanostructures with a He-Cd laser possessing the power approximately 100 W/cm^2, which is represented in the insert of Fig. 3a. That PL spectrum was registered using LabRam HR800 micro-Raman system.

Evolution of DLE and NBE photoluminescence intensities inherent to CdS NCs with rise of the excitation power P_{ex} is exhibited in Fig. 4. As it can be seen, the PL intensity of DLE emission is slowly increased the tendency to saturate with raising the excitation power density, while the intensity of NBE grows superlinearly exceeding the intensity of the DLE emission after some moment (Figs 3 and 4). The insert demonstrates their behavior at low level of the excitation, which is not resolved at the origin of Fig. 4. It is seen that at low level of excitation, both DLE and NBE rise superlinearly.

As the result of competition between the NBE and DLE recombination channels, the emitted color of CdS NCs gradually changes from red to green. Analogous power dependent emission color tunable property was observed in many nanostructures, such as CdS doped with tin, manganese, indium [41–44], SnO$_2$ nanowires [45].

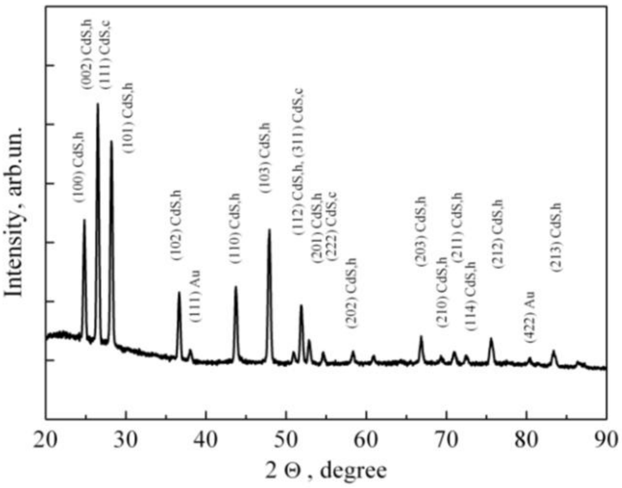

Fig. 2. X-ray diffraction spectra of as-synthesized CdS nanocrystals.

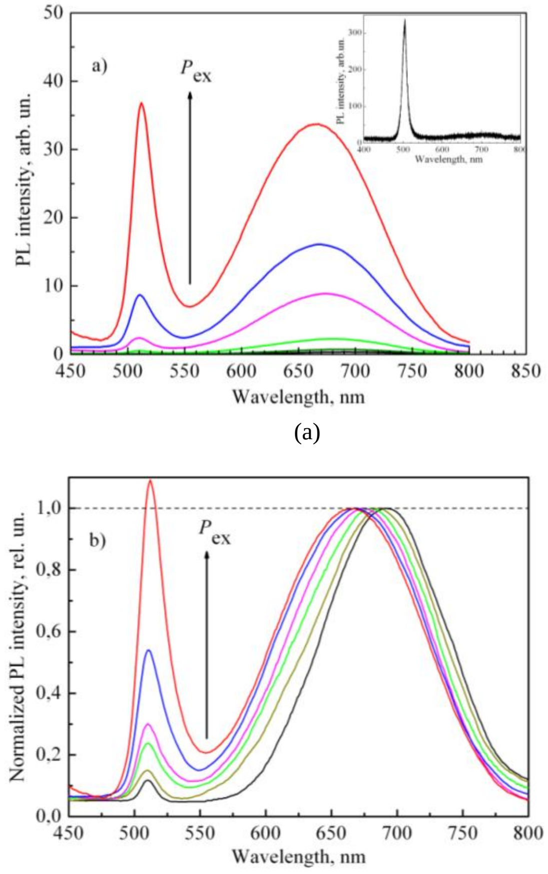

(a)

(b)

Fig. 3. (a) PL spectra of CdS NCs dependence on the excitation power density at room temperature. Insert – PL spectra, at excitation power density 100 W/cm^2; (b) Normalized PL spectra of CdS NCs for various excitation power densities. (Color online.)

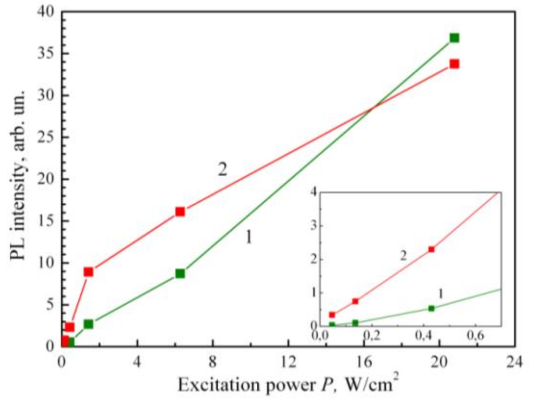

Fig. 4. Dependence of the intensity for NBE (green) (*1*) and DLE (red) (*2*) emissions *versus* the excitation power.

To make clearer the process of luminescence in both bands, these dependences are adduced in the logarithmic scale (Fig. 5a). Both dependences are shown in different scales to avoid their crossing and shadowing of some features at high level of excitation.

It is seen that both dependences behave visually rather similar, but the bend of the DLE dependence for 1.4 W/cm^2 excitation is steeper. The similarity can be explained by the fact that we excite our nanocrystals into conduction band by photons of ~2.64 eV and emission from defect levels arises after the relaxation of electrons from the conduction band on defect levels within the forbidden band. So, the number of electrons in the conduction band and on defect levels should correlate.

In fact, there are a number of different models of possible nonlinearity and the change of the mechanism of nonlinearity of the luminescence with the excitation power [46–49]. They use different assumptions about one or few levels in the band gap. However, even with one defect level in the band gap the system of kinetic equations for such a system demands some simplifications to be solved and there is variety of possible evolution of the nonlinear response of luminescence to the excitation power depending on the model parameters. These changes correspond to the change of the relaxation scheme at the change of the excitation power and, correspondingly, the change of generated carriers and population of different energy levels. For example, Fig. 7 in [48] well corresponds to the linearization shown in Fig. 5b with accounting the bend of dependences shown in Fig. 5a. If to accept this interpretation, and the radiative recombination rate model, where the luminescence intensity I_{PL} corresponds to the dependence [50]

$$I_{PL} = \eta \times P^{\alpha}{}_{excitat} \tag{1}$$

where $P_{excitat}$ is the excitation power and η is the emission efficiency, we have for the exponent α representing the radiative recombination mechanism before and after the bend close values of 1.24 and 1.21, correspondingly for NBE luminescence, while in the transition range between two different relaxation schemes $\alpha = 0.8$. Respectively, for DLE emission this exponent is $\alpha = 0.95$ before the bend close to 1.4 W/cm^2, drops down to 0.4 in the transition region and increases to only 0.62 after the bend for new relaxation scheme. The latter demonstrates that in new relaxation scheme the population of the defect level grows noticeably slower than before, which is exhibited in slow saturation of the intensity of long-wave band. It should be noted that the value of the growth exponent α in the dependence of PL intensity *versus* the excitation power is defined by the dominant carrier recombination process in nanostructure at a given excitation intensity.

On the other hand, errors of measurements do not allow making any unambiguous conclusion about all mechanisms, because of the features inherent to NBE dependence are rather small, and that whole dependence may be interpreted as linear. However, the bend of DLE dependence at the excitation power close to 1.4 W/cm^2 is more pronounced, and it cannot be ignored.

The second linearization scheme is shown in Fig. 4c. The size of symbols corresponds to experimental errors, and one linear approximation of the NBE dependence

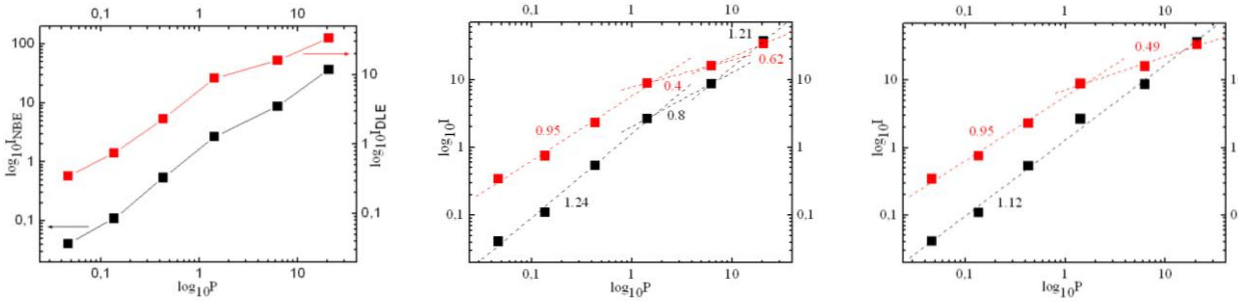

a) b) c)

Fig. 5. Room temperature PL intensities of NBE and DLE emissions as a function of excitation power density P_{ex} (a) and their approximation by three (b) or one/two straight lines (c).

shown in Fig. 4c goes not so close to them as in Fig. 4b, but rather close. In this case for the NBE intensity, we obtained for equation (1) $\alpha = 1.12$. This value is rather close to 1.07 reported for analogous CdS nanowires [36]. These values indicate that the NBE emission should be mainly attributed either to free or bound excitons or bound electron-hole complexes annihilation, while for band-to-band recombination $\alpha = 2$ [51]. DLE dependence can be approximated by two linear dependences with $\alpha = 0.95$ for low excitation and $\alpha = 0.49$ for high excitation levels.

In spite of impossibility to make unambiguous conclusion about carrier dynamics at different excitations, both discussed approaches indicate some slowing of the population of defect levels at the rising excitation power.

In addition to this feature, Fig. 3 demonstrates other details of DLE emission. The rise of FWHM of this band with increasing the excitation power was noticed before, as well as noticeable shift of the maximum to the blue spectral range. The position of peak energy for the DLE band *versus* the excitation power is shown in Fig. 6.

This blue shift of about 65 meV is more pronounced in its value than the red shift of the NBE maximum, which is close to 10 meV. The latter shift may be explained by heating of the sample at the rising excitation power. At the same time, this big shift of DLE band cannot be explained as only visual shift corresponding to approach of the NBE band caused by their mutual overlapping. Thus, we can conclude that the shift of DLE band maximum and increase of its FWHM, which looks similar to asymmetrical widening into the blue range, are defined by some additional mechanism.

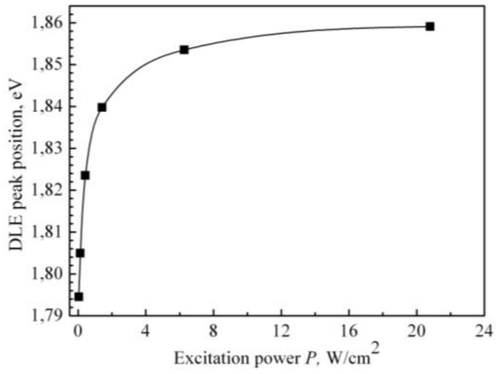

Fig. 6. Dependence of peak position energy for DLE emission on the excitation power density. Solid line – as guided to the eye.

This behavior demonstrates much clear pronounced saturation than that for the intensity of DLE band in Fig. 4. All the features of DLE can be easily explained assuming the finite capacity of defect levels and their energy dispersion, as it is shown schematically in Fig. 7.

The main feature of shown scheme is the finite number of defect levels N_{def} and their indicated energy dispersion. It is clear that filling of those levels is defined by bimolecular process, *i.e.* by the number of free electrons in the conduction band n_c and the number of empty defect levels ($N_{def} - n_d$), where n_d is the number of occupied defect levels. It is obvious that increasing n_d results in filling of defect levels with more and more high energy.

It is possible to demonstrate that independently of the kind of electron recombination from any levels to the valence band (mono-molecular or bi-molecular process, or their mixture, or presence of not shown shallow donors and acceptors), if the rate of filling of defect levels is proportional to $n_c(N_{def} - n_d)$, as it is indicated in Fig. 7, limiting filling of that band at low and high excitation power are $n_d = kn_c$ and $n_d = N_{def}$, correspondingly.

This scheme describes all features of emission from the defect levels. Increasing the excitation power excites more and more electrons to the conduction band and, correspondingly, fills more defect levels with more and more high energy. However, the total filling of defect levels approaches the limiting value N_{def}. As the result, the total intensity of the DLE is saturated, since the maximal number of defect level is limited, and the band shifts to higher energies as the levels with the higher energy contribute to the increasing FWHM of luminescencent band, too. As relatively smaller numbers

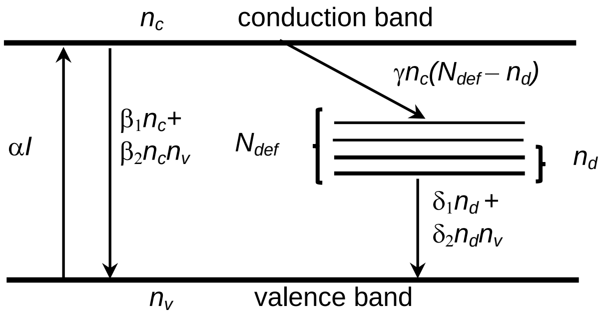

Fig. 7. Possible scheme of defect levels in the bandgap and electron transitions.

of free electrons relax to defect levels at their filling, more electrons participate in NBE emission giving additional contribution into the superlinear dependence of the NBE intensity *versus* the excitation power.

The present analysis can not accurately ascertain the nature of these defect levels; however, the energy of DLE has the maximum in the approximate range 1.77…1.9 eV, which, according to the published data [37, 52, 53, 54], corresponds to surface-related defect states, native defects such as interstitials and vacancies of sulfur or cadmium. This assumption is confirmed by our previous results [32], where the intensity of DLE decreased after annealing of samples in sulfur vapor, which decreases the number of sulfur vacancies. It was noted that the growth of nanocrystals from stoichiometric amount of cadmium and sulfur results in noticeable amount of sulfur vacancies. We demonstrated [32] that the use of gold seeds as the catalyst remarkably increases the speed of the growth of nanocrystals accompanying a remarkable increase of DLE, as compared with nanocrystals grown without any catalyst. We attributed this fact to creation of non-stoichiometric defects, which have no time to be repaired because of fast growth. A large number of defects created due to two noted features of the used synthesis explains creation of narrow defect band resulting in the observed features of DLE.

Another possible origin of the defect levels is twinning interface. It is even proposed as the main reason of DLE in some works [40, 55]. Spectral and structural analyses of CdS nanocrystals synthesized by a two-phase technique showed that the broad low-energy PL emission band from 500 up to 750 nm can be attributed to optical transitions with participation of electronic states induced by twinning interfaces in the nanocrystals [40]. Another investigation [56] demonstrates some influence of the structure on luminescence properties inherent to ensembles just for mesoscopic sizes of crystallites. However, there are no general conclusions about this influence. So, for our samples the question of the influence of polymorphism on investigated optical properties is still open. The general result, which could be expected, is the higher value of FWHM for emission bands in these samples.

4. Conclusions

Our investigations of the excitation power-dependent photoluminescence properties of the ensemble of CdS nanocrystals synthesized using the CVD method have demonstrated the tunable photoluminescence of undoped CdS nanocrystals *with two types of crystal structure,* which can be finely controlled and easily realized, depending on outer excitation power and native defect concentration.

The luminescent properties of the CdS nanocrystals demonstrate competition of different relaxation mechanisms resulting in different power dependence of NBE and DLE emission *versus* the excitation power and their variation during the rise of the excitation power. As a result, luminescence of CdS nanocrystals changes its color under changing the excitation power. Possible mechanisms of this behavior have been discussed, and possible origin of defect levels has been proposed.

The results suggest that this kind of CdS nanocrystals can be applied in the industry of optoelectronic nanodevices.

Acknowledgements

This work was supported by the National research foundation of Ukraine, project 2020/01/0504.

References

1. Li L., Lou Z., Shen G. Hierarchical CdS nanowires based rigid and flexible photodetectors with ultrahigh sensitivity. *ACS Appl. Mater. Interfaces*. 2015. **7**. P. 23507–23514. https://doi.org/10.1021/acsami.5b06070.
2. Gu Y., Kwak E.S., Lensch J.L. *et al.* Near-field scanning photocurrent microscopy of a nanowire photodetector. *Appl. Phys. Lett.* 2005. **87**. Art. No 043111. https://doi.org/10.1063/1.1996851.
3. Huang Y., Duan X., Lieber C.M. Nanowires for integrated multicolor nanophotonics. *Small.* 2005. **1**. P. 142–147. https://doi.org/10.1002/smll.200400030.
4. Bao R., Wang C., Dong L. *et al.* CdS nanorods/organic hybrid LED array and the piezo-phototronic effect of the device for pressure mapping. *Nanoscale.* 2016. **8**, No 15. P. 8078–8082. https://doi.org/10.1039/c6nr00431h.
5. Couteau C., Larrue A., Wilhelm C., Soci C. Nanowire lasers. *Nanophoton*. 2015. **4**, No 1. P. 90–107. https://doi.org/10.1515/nanoph-2015-0005.
6. Garnett E.C., Brongersma M.L., Cui Y., McGehee M.D. Nanowire solar cells. *Annu. Rev. Mater. Res.* 2011. **41**. P. 269–295. https://doi.org/10.1146/annurev-matsci-062910-100434.
7. Brenneman K.L., Poduri S., Stroscio M.A., Dutta M. Optical detection of lead (II) ions using DNA-based nanosensor. *IEEE Sensor Journal.* 2013. **13**, No 5. P. 1783–1786. https://doi.org/10.1109/JSEN.2013.2241757.

8. Zhu L., Feng C., Li F. *et al.* Excellent gas sensing and optical properties of single-crystalline cadmium sulfide nanowires. *RSC Adv*. 2014. **4**. P. 61691–61697. https://doi.org/10.1039/C4RA11010B.
9. Mu L., Chang Y., Sawtelle S.D. *et al.* Silicon nanowire field-effect transistors – A versatile class of potentiometric nanobiosensors. *IEEE Access*. 2015. **3**. P. 287–302. https://doi.org/10.1109/access.2015.2422842.
10. Kind H., Yan H., Messer B., Law M., Yang P. Nanowire ultraviolet photodetectors and optical switches. *Adv. Mater*. 2002. **14**, No 2. P. 158–160. https://doi.org/10.1002/1521-4095.
11. Gazquez G.C, Lei S., George A. *et al*. Low-cost, large-area, facile, and rapid fabrication of aligned ZnO nanowire device arrays. *ACS Appl. Mater. Interfaces*. 2016. **8**. P. 13466–13471. https://doi.org/10.1021/acsami.6b01594.
12. Liang Y., Liang H., Xiao X., Hark S. The epitaxial growth of ZnS nanowire arrays and their applications in UV-light detection. *J. Mater. Chem.* 2012. **22**, No 3. P. 1199–1205. https://doi.org/10.1039/c1jm13903g.
13. Zhang X., Liu Q., Liu B. *et al.* Giant UV photoresponse of a GaN nanowire photodetector through effective Pt nanoparticle coupling. *J. Mater. Chem*. C. 2017. **5**. P. 4319–4326. https://doi.org/10.1039/C7TC00594F.
14. Yan X., Li B., Wu Y., Zhang X., Ren X. A single crystalline InP nanowire photodetector. *Appl. Phys. Lett*. 2016. **109**. Art. No 053109. https://doi.org/10.1063/1.4960713.
15. Gomes U.P., Ercolani D., Zannier V., Beltram F., Sorba L. Controlling the diameter distribution and density of InAs nanowires grown by Au-assisted methods. *Semicond. Sci. Technol*. 2015. **30**. Art. No 115012. https://doi.org/10.1088/0268-1242/30/11/115012.
16. Madelung O., Schulz M., Weiss H. *Semiconductor Physics of Group II VI Compounds; New Series, Group III*. Berlin, Landolt-Bornstein, 1982. https://doi.org/10.1007/b71137.
17. Heo K., Lee H., Park Y. *et al.* Aligned networks of cadmium sulfide nanowires for highly flexible photodetectors with improved photoconductive responses. *J. Mater. Chem*. 2012. **22**. P. 2173–2179. https://doi.org/10.1039/c2jm14359c.
18. Shen G., Cho J.H., Yoo J.K., Yi G.-C., Lee C.J. Synthesis of single-crystal CdS microbelts using a modified thermal evaporation method and their photoluminescence. *J. Phys. Chem. B.* 2005. **109**. P. 9294–9298. https://doi.org/10.1021/jp044888f.
19. Poduri S., Dutta M., Stroscio M. Photoluminescence characterization of cadmium sulphide (CdS) nanowires for polarization studies. *Appl. Phys. Res.* 2017. **9**, No 6. P. 26–35. https://doi.org/10.5539/apr.v9n6p26.
20. Poduri S., Dutta M., Stroscio M. Characterization of CdS nanowires self-assembled in a nanoporous alumina template. *J. Electronic Mater*. 2014. **43**, No 11. P 3979–3983. https://doi.org/10.1007/s11664-014-3305-0.
21. Geburt S., Thielmann A., Röder R. *et al.* Low threshold room-temperature lasing of CdS nanowires. *Nanotechnology*. 2012. **23.** Art. No 365204. https://doi.org/10.1088/0957-4484/23/36/365204.
22. Jang J.S., Joshi U.A., Lee J.S. Solvothermal synthesis of CdS nanowires for photocatalytic hydrogen and electricity production. *J. Phys. Chem. C.* 2007. **111**. P. 13280–13287. https://doi.org/10.1021/jp072683b.
23. Alkuam E., Badradeen E., Guisbiers G. Influence of CdS morphology on the efficiency of dye-sensitized solar cells. *ACS Omega.* 2018. **3**. P. 13433–13441. https://doi.org/10.1021/acsomega.8b01631.
24. Law M., Goldberger J., Yang P. Semiconductor nanowires and nanotubes. *Ann. Rev. Mater. Res*. 2004. **34**. P. 83–122. https://doi.org/10.1146/annurev.matsci.34.040203.112300.
25. Li D., Liu Y., de la Mata M. *et al.* Strain-induced spatially indirect exciton recombination in zinc-blende/wurtzite CdS heterostructures. *Nano Res*. 2015. **8**, No 9. P. 3035–3044. https://doi.org/10.1007/s12274-015-0809-8.
26. Liu R.B., Zhuang X.J., Xu J.Y. *et al.* Trap-state whispering-gallery mode lasing from high-quality tin-doped CdS whiskers. *Appl. Phys. Lett*. 2011. **99**, No 26. P. 263101. https://doi.org/10.1063/1.3672032.
27. Wei S.-H., Zhang S.B. Structure stability and carrier localization in CdX (X = S, Se, Te) semiconductors. *Phys. Rev. B.* 2000. **62**, No 11. P. 6944–6947. https://doi.org/10.1103/physrevb.62.6944.
28. Zhang Q., Xing X., Zhou X., Xiong X., Zhai T. Stoichiometric effect on optoelectronic properties of composition-tunable $CdS_{1-x}Se_x$ nanowires. *Adv. Opt. Mater*. 2017. **5**, No 5. Art. No 1600877. https://doi.org/10.1002/adom.201600877.
29. Zhu J., Jiang W., Wang B. *et al.* Highly efficient wurtzite/zinc blende CdS visible light photocatalyst with high charge separation efficiency and stability. *J. Chem. Phys*. 2020. **152**. Art. No 244703. https://doi.org/10.1063/5.0011132.
30. Ghosh A., Paul S., Raj S. Structural phase transformation from wurtzite to zinc-blende in uncapped CdS nanoparticles. *Solid State Commun*. 2013. **154**. P. 25–29. https://doi.org/10.1016/j.ssc.2012.10.038.
31. Zhou Z., Li M., Wu P., Guo L. Revisiting the zinc-blende/wurtzite heterocrystalline structure in CdS. *Adv. Condens. Matter Phys*. 2014. **2014**. P. 1–7. https://doi.org/10.1155/2014/361328.
32. Bogoslovskaya A.B., Grynko D.O., Bortchagovsky E.G., Gudymenko O.I. Luminescent analysis of the quality of CdS nanocrystals depending on technological parameters. *Semiconductor Physics, Quantum Electronics and Optoelectronics*. 2019. **22**. P. 231–236. https://doi.org/10.15407/spqeo22.02.231.

33. Grynko D.A., Fedoryak A.N., Dimitriev O.P. *et al.* Growth of CdS nanowire crystals: Vapor–liquid–solid versus vapor–solid mechanisms. *Surf. Coatings Technol*. 2013. **230**. P. 234–238. https://doi.org/10.1016/j.surfcoat.2013.06.058.
34. Georgobiani A.N., Sheynkman M.K. *The Physics of* $A^{II}B^{VI}$ *Compounds*. Moscow, Nauka, 1986 (in Russian).
35. Bogoslovskaya A.B., Khalimovskyy O.M., Grynko D.O. Piezo-mechanical impedance of nanosized CdS single crystal. *Semiconductor Physics, Quantum Electronics and Optoelectronics*. 2019. **22.** P. 479–485. https://doi.org/10.15407/spqeo22.04.479.
36. Gao X., Pang G., Ni Z., Chen R. Surface-related exciton and lasing in CdS nanostructures. *Nanoscale Res. Lett.* 2019. **14**, No 1. Art. No 216. https://doi.org/10.1186/s11671-019-3036-5.
37. Agata M., Kurase H., Hayashi S., Yamamoto K. Photoluminescence spectra of gas-evaporated CdS microcrystals. *Solid State Commun*. 1990. **76**, No 8. P. 1061–1065. https://doi.org/10.1016/0038-1098(90)90084-O.
38. Liu B., Chen R., Xu X.L. *et al.* Exciton-related photoluminescence and lasing in CdS nanobelts. *J. Phys. Chem. C*. 2011. **115**, No. 26. P. 12826–12830. https://doi.org/10.1021/jp203551f.
39. Veamatahau A., Jiang B., Seifert T. *et al.* Origin of surface trap states in CdS quantum dots: Relationship between size dependent photoluminescence and sulfur vacancy trap states. *Phys. Chem. Chem. Phys*. 2015. **17**, No 4. P. 2850–2858. https://doi.org/10.1039/c4cp04761c.
40. Zhao P.Q., Xiong S.J., Wu X.L., Chu P.K. Photoluminescence induced by twinning interface in CdS nanocrystals. *Appl. Phys. Lett*. 2012. **100**. Art. No 171911. https://doi.org/10.1063/1.4707388.
41. Guo S., Zhao F.Y., Li Y. *et al.* Individual dual-emitting CdS multi-branched nanowire arrays under various pumping powers, *Appl. Phys. Lett.* 2016. **109**. Art. No 162101. https://doi.org/10.1063/1.4964879.
42. Zhang L., Liu R., Zou B. Sn-doped CdS nanowires with low temperature lasing by CW-laser excitation. *ACS Appl. Electron. Mater*. 2020. **2**. P. 282–289. https://doi.org/10.1021/acsaelm.9b00766.
43. Chen O., Shelby D.E., Yang Y. *et al.* Excitation-intensity-dependent color-tunable dual emissions from manganese-doped CdS/ZnS core/shell nanocrystals. *Angew. Chem. Internat. Ed.* 2010. **49**. P. 10132–10135. https://doi.org/10.1002/anie.201004926.
44. Xu J., Quan S., Zou Z. *et al.* Color-tunable photoluminescence from In-doped CdS nanowires. *Chem. Phys. Lett.* 2016. **652**. P. 216–219. https://doi.org/10.1016/j.cplett.2016.04.068.
45. Liu R., Chen Y., Wang F. *et al.* Stimulated emission from trapped excitons in SnO_2 nanowires. *Phys. E: Low-Dimens. Syst. Nanostruct.* 2007. **39**. P. 223–229. https://doi.org/10.1016/j.physe.2007.04.009.
46. Duboc C.A. Nonlinearity in photoconducting phosphors. *Brit. J. Appl. Phys*. 1955. **6**, No S4. P. S107–S111. https://doi.org/10.1088/0508-3443/6/S4/343.
47. Bube R.H. Analysis of photoconductivity applied to cadmium-sulfide-type photoconductor. *J. Phys. Chem. Solids*. 1957. **1**. P. 234–248. https://doi.org/10.1016/0022-3697(57)90012-4.
48. Klasens H.A. The intensity-dependence of photoconduction and luminescence of photoconductors in the stationary state. *J. Phys. Chem. Solids.* 1958. **7**. P. 175–200. https://doi.org/10.1016/0022-3697(58)90260-9.
49. Reshchikov M.A., Olsen A.J., Bishop M.F., McMullen T. Superlinear increase of photoluminescence with excitation intensity in Zn-doped GaN. *Phys. Rev. B*. 2013. **88**. Art. No 075204. https://doi.org/10.1103/PhysRevB.88.075204.
50. Pankove J.I. *Optical Processes in Semiconductors.* New York, Dover, 1971.
51. Fouquet J.E., Siegman A.E. Room-temperature photoluminescence times in a $GaAs/Al_xGa_{1-x}As$ molecular beam epitaxy multiple quantum well structure. *Appl. Phys. Lett*. 1985. **46**, No 3. P. 280–282. https://doi.org/10.1063/1.95658.
52. Vigil O., Riech I., Garcia-Rocha M., Zelaya-Angel O. Characterization of defect levels in chemically deposited CdS films in the cubic-to-hexagonal phase transition. *J. Vac. Sci. Technol. A*. 1997. **15**, No 4. P. 2282–2286. https://doi.org/10.1116/1.580735.
53. Wang C., Ip K.M., Hark S.K., Li Q. Structure control of CdS nanobelts and their luminescence properties. *J. Appl. Phys*. 2005. **97**, No 5. Art. No 054303. https://doi.org/10.1063/1.1852094.
54. Wang Z.Q., Gong J.F., Duan J.H. *et al.* Direct synthesis and characterization of CdS nanobelts. *Appl. Phys. Lett*. 2006. **89**. Art. No 033102. https://doi.org/10.1063/1.2222237.
55. Torres-Castanedo C.G., Márquez-Marín J., Castanedo-Pérez R. *et al.* Optical properties of CdS nanocrystalline thin films in the abrupt phase transition from zinc blende to wurtzite. *J. Mater. Sci.: Mater. Electron*. 2020. **31**. P. 16561–16568. https://doi.org/10.1007/s10854-020-04211-y.
56. Bergman L., Chen X.-B., Morrison J.L., Huso J., Purdy A.P. Photoluminescence dynamics in ensembles of wide-band-gap nanocrystallites and powders. *J. Appl. Phys*. 2004. **96**, No 1. P. 675–682. https://doi.org/10.1063/1.1759076.

Authors' contributions

A. Bogoslovska: conceptualization, investigation, formal analysis, writing – original draft, writing – review & editing.

D. Grynko: resources, writing – review & editing.

E. Bortchagovsky: formal analysis, writing – review & editing, project administration.

Authors and CV

Alla Bogoslovskaya, Senior scientific researcher at the Department of Physics of Optoelectronic Devices, V. Lashkaryov Institute of Semiconductor Physics, NASU. The area of scientific interests includes physics and technology of semiconductor nanostructured materials and device structures of optoelectronics. Authored over 60 publications. https://orcid.org/0000-0003-2056-1430

Bortchagovsky Eugene, born in 1959, he defended his Ph.D. thesis in Semiconductor Physics in 1991 at the Moscow State University and Dr.Sci. in Physics in the field of Optics in 2016 at the Institute of Physics of NASU. He is senior researcher and head of a laboratory at the V. Lashkaryov Institute of Semiconductor Physics, NASU. He is the author of over 75 articles in peer reviewed journals. The area of his scientific interests includes plasmonics, near-field optics, ellipsometry. E-mail: bortch@yahoo.com;
http://orcid.org/0000-0001-7742-9655.

Dmytro Grynko, Senior researcher at the Department of Functional Materials and Nanostructures (*laboratory of the optoelectronic molecular-semiconducting systems*) at the V. Lashkaryov Institute of Semiconductor Physics, National Academy of Sciences of Ukraine. Scope of current research interests: functional molecular, low-dimensional nanostructures and nanocomposite nanostructured thin film media, gas-phase technology and application, template guided self-organization, technology of low-dimensional structures, nano-sized single crystals. Technical experience: nanowires, nano-sized single crystals growth from gas-phase; gas-phase technology for multicomponent nanocomposites films based on fullerenes, organic dyes, organic polymer and inorganic compounds; CVD, organometallic compounds.
http://orcid.org/0000-0002-1890-4222

Люмінесцентні властивості нанокристалів сульфіду кадмію, вирощених з газової фази

А.Б. Богословська, Д.О. Гринько, Є.Г. Борщагівський

Анотація. Досліджено фотолюмінесцентні властивості нелегованих нанокристалів сульфіду кадмію в залежності від потужності збудження. Спектри фотолюмінесценції нанокристалів CdS, вирощених із газової фази, виміряні при кімнатній температурі, виявили дві смуги випромінювання: з положеннями максимумів при 510 нм (крайове випромінювання) та приблизно при 690 нм (глибокі дефектні рівні). Продемонстровано регульовану потужністю збудження фотолюмінесценцію нанокристалів CdS із зміною основного випромінювального каналу від релаксації через рівні дефектів до прямої крайової релаксації, що приводить до зміни кольору. Обговорюється нелінійна поведінка інтенсивності ліній випромінювання обох смуг, а також зсув піку випромінювання дефектної смуги в синю сторону, що пояснюється скінченною ємністю підзони дефектів у забороненій зоні. Походження випромінювання довгохвильової смуги пов’язане з природними дефектами, такими як вакансії сірки або двійникування на границях зерен.

Ключові слова: CdS, нанокристали, фотолюмінесценція, морфологія кристала, потужність збудження.